Nanoscale

Enhanced magnetism in lightly doped manganite heterostructures: strain or stoichiometry?

Journal:	*Nanoscale*
Manuscript ID	NR-ART-11-2018-009693.R1
Article Type:	Paper
Date Submitted by the Author:	15-Feb-2019

Complete List of Authors:	Mbatang, Richard; New Mexico State University Xue, Deqing; State Key Laboratory for Mechanical Behavior of Materials, Xi'an Jiaotong University, Xi'an 710049, China Enriquez, Erik; University of Texas at San Antonio, Physics and Astronomy Yuan, Ruihao; Los Alamos National Laboratory Han, Hyungkyu; Univerzita Palackeho Prirodovedecka Fakulta, Dowden, Paul; Los Alamos National Laboratory Wang, Qiang; West Virginia State University Fohtung, Edwin; New Mexico State University Xue, Dezhen; Xi'an Jiaotong University Lookman, Turab; Theoretical Division and Center for Nonlinear Studies, Los Alamos National Laboratory,, Pennycook, Stephen J. ; National University of Singapore, Department of Materials Science and Engineering Chen, Aiping; Los Alamos National Laboratory, Center for Integrated Nanotechnologies (CINT)

SCHOLARONE™
Manuscripts

Please do not adjust margins

Journal Name

ARTICLE

Enhanced magnetism in lightly doped manganite heterostructures: strain or stoichiometry?

Received 00th Dec 2018,
Accepted 00th January 20xx

DOI: 10.1039/x0xx00000x

www.rsc.org/

Richard Mbatang,[†,a,b] Deqing Xue,[†,c,d] Erik Enriquez,[a] Ruihao Yuan,[e] Hyungkyu Han,[a,e] Paul Dowden,[a] Qiang Wang,[f] Edwin Fohtung,[b] Dezhen Xue,[c] Truab Lookman,[e] Stephen J. Pennycook,[*,d] and Aiping Chen[*,a]

Lattice mismatch induced epitaxial strain has been widely used to tune functional properties in complex oxide heterostructures. Apart from the epitaxial strain, a large lattice mismatch also produces other effects including modulations in microstructure and stoichiometry. However, it is challenging to distinguish the impact of these effects from the strain contribution to thin film properties. Here, we use $La_{0.9}Sr_{0.1}MnO_3$ (LSMO), a lightly doped manganite close to the vertical phase boundary, as a model system to demonstrate that both epitaxial strain and cation stoichiometry induced by strain relaxation contribute to functionality tuning. The thinner LSMO films are metallic with a greatly enhanced T_C which is 97 K higher than the bulk value. Such anomalies in T_C and transport cannot be fully explained by the epitaxial strain alone. Detailed microstructure analysis indicates La deficiency in thinner films and twin domains formation in thicker films. Our results have revealed that both epitaxial strain and strain relaxation induced stoichiometry/microstructure modulations contribute to the modified functional properties in lightly doped manganite perovskite thin films.

1. Introduction

Epitaxial strain induced by lattice mismatch is one of the most fascinating approaches to control functional properties in complex oxide heterostructures. A variety of physical properties such as magnetoresistance, magnetic anisotropy, superconductivity, ionic conduction and electric polarization have been manipulated by strain engineering.[1-3] Among these materials, doped manganite perovskites have attracted much interest due to the various structural, magnetic and transport properties observed at different temperatures with change in the dopant concentration.[4, 5] Strain engineering has been applied in different manganite perovskites for tuning physical properties in both lateral heterostructures [6-9] and vertical nanocomposites.[10] Strain tunes physical properties via modifying the Mn-O-Mn bond length and angle and MnO_6 octahedral rotation. It has been shown that compressive strain tends to enhance the magnetic and transport properties of manganite thin films while tensile strain suppresses ferromagnetism by reducing T_C due to the distortion of the MnO_6 octahedra.

In a metal system, the strain-stress curve follows an elastic deformation before the plastic deformation and fracture. The upper limiting strain of the elastic deformation varies significantly in different metals (0.5%~2%). In ceramic oxide thin films, such an upper limit threshold for the elastic deformation has not been adequately explored. In epitaxial heterostructures, the lattice parameter change has often been defined as the strain, which has been used as the main parameter for physical properties tuning. However, there are two critical questions: 1) does the lattice parameter difference reflect a true elastic strain and 2) does the epitaxial strain alone modify the physical properties or other factors induced by strain relaxation also contribute to modified functionalities? First of all, the lattice parameter of perovskite oxide films is strongly tied to the cation and anion stoichiometry. A strong dependence of out-of-plane lattice parameter on oxygen pressure and laser energy density is reported in a variety of complex oxides confirms that such a lattice parameter variation may not be fully induced by the elastic deformation.[11, 12] In addition, when the misfit strain is larger than the elastic strain upper limit, strain tends to relax which induces a variety of other effects that could impact the

[a] Center for Integrated Nanotechnologies (CINT), Los Alamos National Laboratory, Los Alamos, New Mexico 87545, USA
[b] Department of Physics, New Mexico State University, Las Cruces, New Mexico 88003, USA
[c] State Key Laboratory for Mechanical Behavior of Materials, Xi'an Jiaotong University, Xi'an 710049, China
[d] Department of Materials Science and Engineering, National University of Singapore, Singapore 117575, Singapore
[e] Theoretical Division, Los Alamos National Laboratory, Los Alamos, New Mexico 87545, USA
[f] Department of Physics and Astronomy, West Virginia University, Morgantown, West Virginia 26506, USA
† These authors contributed to this work equally.
* Email: steve.pennycook@nus.edu.sg; apchen@lanl.gov

Electronic Supplementary Information (ESI) available: [details of any supplementary information available should be included here]. See DOI: 10.1039/x0xx00000x

Please do not adjust margins

physical properties. Besides misfit dislocations, other mechanisms including microstructure modulation, cation stoichiometry modulation and defect modulation have been reported for strain relaxation. For example, oxygen vacancy formation/ordering and La accumulation have been reported in oxide heterostructures and vertical nanocomposites for strain relaxation.[13, 14] Owing to the complex strain relaxation mechanisms, how these factors contribute to modified physical properties is not clear.

In optimum doped manganite thin films, T_C is not extremely sensitive to doping concentration as evidenced by the plateau in the phase diagram. Therefore, the effect of a small composition variation in optimum doped manganite thin films can be easily shadowed by strain effects. To explore the roles of other factors such as strain relaxation induced microstructure and stoichiometry modulations, we chose lightly doped $La_{0.9}Sr_{0.1}MnO_3$. This compound is close to the vertical phase boundary and exhibits interesting magnetic phase transition and structural transition which are extremely sensitive to both strain and stoichiometry. The lightly doped manganites have been widely studied in bulk form due to coupling among lattice, spin and orbital degrees of freedom.[15-18] For example, two ferromagnetic phases have been predicted in lightly doped $La_{1-x}Sr_xMnO_3$.[19] Static pressure modifies charge ordering, metal insulator transition (MIT) temperature (T_{MI}), and Curie temperature (T_C).[20-22] The effects in these lightly doped manganite thin films are often controversial,[23-26] largely because the film growth of lightly doped manganite is sensitive to growth conditions.[27] For example, high temperature growth and long annealing could promote strong interdiffusion which makes the modified properties ambiguous. In addition, the impact of cation stoichiometry, depending on growth conditions, is rarely discussed in lightly doped manganite films. Therefore, the enhanced magnetism and transport properties in lightly doped $La_{1-x}Sr_xMnO_3$ manganite thin films is still not clear. In fact, the anomalies of magnetism and transport are not limited to Sr doped $LaMnO_3$, it has been observed in $LaMnO_3$ and Ba doped $LaMnO_3$.[28, 29] In this study, we investigated why the magnetism and transport of the lightly doped manganite $La_{0.9}Sr_{0.1}MnO_3$ thin films are completely different from the bulk counterpart. By changing the film thickness, strain relaxation mechanisms were observed including La off-stoichiometry, twin domain tilting and misfit dislocation formation. We found out that epitaxial strain and strain relaxation modulated cation off-stoichiometry and microstructure are responsible for the modified T_C, T_{MI} and electron transport, compared to the bulk counterpart.

2. Results and Discussion

$La_{0.9}Sr_{0.1}MnO_3$ (LSMO) bulk is orthorhombic with room temperature lattice parameters of a = 5.5469 Å, b = 5.5603 Å, and c = 7.7362 Å.[30] The pseudocubic lattice parameters are given by a_0 = 3.922 Å, b_0 = 3.932 Å, c_0 = 3.868 Å. Bulk $La_{0.9}Sr_{0.1}MnO_3$ is a ferromagnetic insulator with a Curie temperature (T_C) of 145 K, a charge ordering temperature (T_{CO}) of 127 K and a saturation magnetization of 3.6 μ_B/Mn.[4] A lattice mismatch of -3.4% exists between LSMO and $LaAlO_3$ (3.789 Å) substrate. Figure 1(a) shows a local 2ϑ-ω scan of LSMO films with different thicknesses. No extra peaks were observed on the 2ϑ-ω full scan (not shown here). Only the (00*l*) peaks of the film and the substrate were observed indicating the growth of highly oriented LSMO films on LAO substrates. With decreasing film thickness, the out-of-plane lattice parameter increases from 3.885 Å (95 nm film) to 3.929 Å (15 nm film). To understand the in-plane strain states, reciprocal space mapping (RSM) of these three films was conducted at LAO (103) peak region. Figures 1(b)-1(d) show RSM (103) of 15 nm, 30 nm and 95 nm, respectively. An in-plane lattice parameter of 3.865 Å and 3.876 Å was found for the 15 nm and 30 nm films, respectively. The 95 nm film shows Bragg peak splitting which is related to the formation of large twin domains driven by shear strain relaxation.[31-33] An in-plane lattice parameter of 3.910 Å (square yellow box in Figure 1d) was found for the 95 nm film. The in-plane strain, out-of-plane strain and Poisson's ratio are shown in Table 1. Poisson's ratio of thinner films is ~0.33 which is in agreement with perovskite manganites.[34, 35] Similar twin formation has been observed in compressively strained $BiFeO_3$ and $La_{0.7}Sr_{0.3}MnO_3$ films which in bulk have monoclinic and distorted rhombohedral structures, when grown on cubic substrates.[33, 36-38]

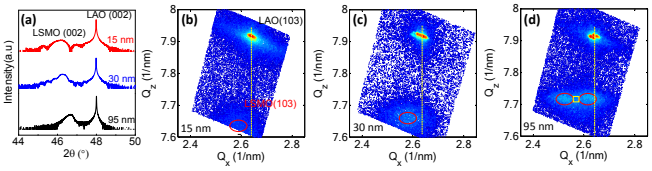

Figure 1. (a) Local 2θ-ω scans of $La_{0.9}Sr_{0.1}MnO_3$ thin films with different thicknesses. (b) Reciprocal space maps of (b) 15 nm, (c) 30 nm and (d) 95 nm LSMO thin films. The color map shows X-ray intensity from high to low (red→green→blue). The circle represents the peak position.

	a (Å)	c (Å)	ε_{xx} (%)	ε_{yy} (%)	ε_{zz} (%)	v	V (cm^3)	T_c (K)	T_{MI} (K)	T_{co} (K)
15 nm	3.865	3.929	-1.453	-1.704	1.577	0.329	58.692	242	250	112
30 nm	3.876	3.920	-1.173	-1.424	1.344	0.337	58.892	200	204	90
95 nm	3.910	3.885	-0.306	-0.559	0.439	0.333	59.394	95	-	-

Table 1: Summary of the 15 nm, 30 nm and 95 nm samples. $\varepsilon_{xx} = (a - a_0) / a_0$, $\varepsilon_{yy} = (a - b_0) / b_0$, $\varepsilon_{zz} = (c - c_0) / c_0$, $v = 1 / (1 - (\varepsilon_{xx} + \varepsilon_{yy}) / \varepsilon_{zz}))$. a and c are the in-plane and out-of-plane lattice parameters of LSMO films. The unit cell volume of bulk LSMO is 59.650 cm^3.

To confirm the microstructure evolution and strain relaxation with film thickness, high-angle annular dark-field (HAADF) scanning transmission electron microscopy (STEM) images were collected for two films. Figure 2(a) shows a high resolution HADDF-STEM image of the 15 nm LSMO on LAO substrate. Misfit dislocations are visible near to the film-substrate interface as highlighted by the red circles, due to the large lattice mismatch (-3.4%). Figures 2(b)-2(f) show the local electron energy loss spectroscopy (EELS) mappings, which show that the film/substrate interface is reasonably sharp without significant interdiffusion. Figure 2(g) shows a cross-sectional TEM image of the 95 nm film. The vertical contrast indicates the formation of twin

This journal is © The Royal Society of Chemistry 20xx

domains as suggested by the XRD results. The domain widths roughly agree with the above estimates from the domain matching epitaxy. Misfit dislocations are also visible at the film-substrate interface of this film as shown in Figure 2(h). To explore the misfit dislocation distribution and the strain relaxation at the interface, we applied geometric phase analysis (GPA). Figures 2(i) and 2(j) show the in-plane lattice strain map ε_{xx} for the 15 nm film and the 95 nm film, respectively. This strain map provides the local lattice displacement with respect to a reference LAO substrate.[39] Misfit dislocations are marked in circles. Their spacing is measured to be about 22 nm in Figure 2(i) and also in fast Fourier transform images (Figure S1a-b) for the 15 nm film. The misfit dislocation spacing is estimated to be ~5.5 nm by considering $d_s = \frac{(a_0 \times a_s)}{2(a_0 - a_s)}$ for complete strain relaxation. Such a significantly increased dislocation spacing indicates that the strain is only partially relaxed. Misfit dislocations in the 95 nm film, as shown in Figure 2(k), have an average spacing of about 23 nm, which is similar with the spacing in the thinner film. In the LSMO/STO system, it was reported that periodic twinning was formed in thinner films while twin domain tilting occurred in thicker films.[31] For these LSMO films on LAO substrates, except misfit dislocations, the strain is mainly relaxed by tilted twin domains formation in thick films.

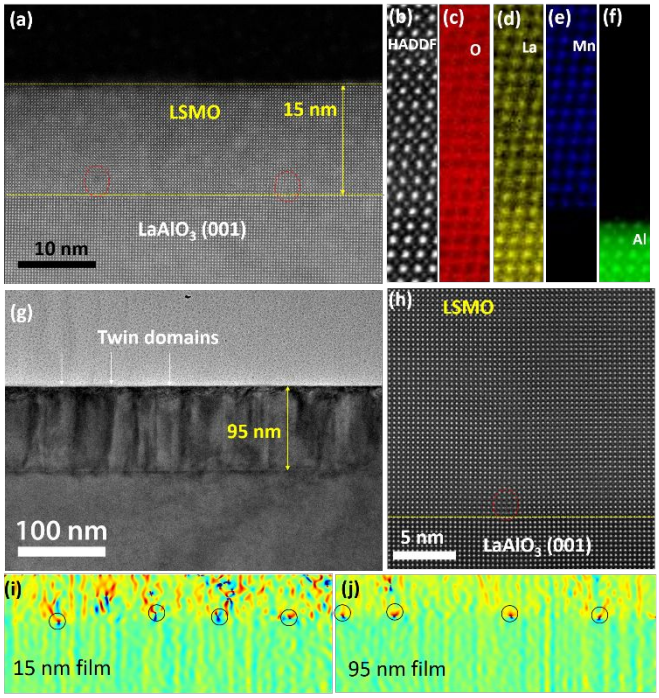

Figure 2. (a) High resolution HAADF STEM image of the 15 nm LSMO film on LAO substrate. (b) HAADF and corresponding EELS mapping of (c) O, (d) La, (e) Mn, and (f) Al. (g) TEM image of the 95 nm LSMO/LAO heterostructure. (h) HAADF STEM image at the film/substrate interface of the 95 nm sample. (h) In-plane lattice strain map ε_{xx} by GPA in (i) 15 nm and (j) 95 nm LSMO/LAO heterostructures. The circles highlight misfit dislocations at the film-substrate interface.

To understand the strain effect on magnetic properties, AC susceptibility was measured in a 10 Oe AC magnetic field at a frequency of 5 kHz to probe the magnetic phase transition. The peak of the real part of the magnetic susceptibility in Figure 3(a) shows T_C of 240 K, 200 K and 82 K for 15 nm, 30 nm and 95 nm samples respectively. The reduced T_c could be related to the complex strain effect from the twin domains as observed in TEM. A reference sample grown on STO with fully relaxed strain show a T_c of 145K (not shown here). The imaginary part of the magnetic susceptibility shows two different peaks in Figure 3(b). A cusp is observed at higher temperatures which coincides with the T_C. The peak at about 40 K is observed at all samples which is attributed to the 'domain' freezing of the tweed structure in the LAO substrate.[40] The enhancement in T_C in thinner films can be related to the large in-plane compressive strain, which elongates the MnO_6 octahedron in the out-of-plane direction and modifies Jahn-Teller distortions. Compressing the MnO_6 in the in-plane direction reduced the bond length that leads to an increase in the in-plane transfer integral or hoping probability. T_C is strain dependent with $T_C(\varepsilon_B, \varepsilon^*) = T_C(0, 0)(1 - \alpha\varepsilon_B - \beta\varepsilon^{*2})$.[32] The bulk compression $\varepsilon_B = (\varepsilon_{xx} + \varepsilon_{yy} + \varepsilon_{zz})/3$ and the biaxial (Jahn-Teller) distortion $\varepsilon^* = (2\varepsilon_{zz} - \varepsilon_{xx} - \varepsilon_{yy})/4$.[41] $\alpha = (1/T_C)dT_C/d\varepsilon_B$ is related to the unit cell volume variations under strain $\varepsilon_B = (1/3)\,\Delta V/V$ and β accounts for the Jahn-Teller energy splitting.[42] For substrate induced biaxial distortion, tensile strain tends to reduce T_C while compressive strain can increase it. It predicts that ~1% biaxial strain produces ~10% shift in T_C in $La_{0.83}Sr_{0.17}MnO_3$.[41] The biaxial distortion induced T_C reduction in optimized doped perovskite manganites also follows the Millis' equation.[35] Interestingly, the biaxial strain in 15 (30) nm films is 1.6% (1.3%) while T_C increases by 66% (37%), respectively. If Millis' equation holds in our samples, the T_C enhancement is far larger than the prediction. $La_{0.9}Sr_{0.1}MnO_3$ is located at the vertical phase boundary region and T_C of these lightly doped manganites is extremely sensitive to the stoichiometry. As shown in the T_C *vs* Sr composition plot,[4] the T_C of $La_{0.9}Sr_{0.1}MnO_3$ is 145 K while the T_C of $La_{0.85}Sr_{0.15}MnO_3$ is 240 K. A simple linear projection indicates that 1% of La or Sr composition change shifts T_C by 19 K. We suspect that other factors such as cation off-stoichiometry along with the biaxial strain contribute to the T_C enhancement.

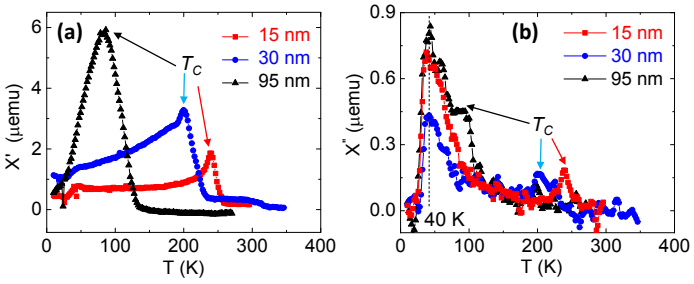

Figure 3. (a) AC χ'-T and (b) χ''-T curves measured in a 10 Oe AC magnetic field at a frequency of 5 kHz for 15 nm, 30 nm and 95 nm LSMO films.

Besides T_C, the electron transport properties have also been significantly modified. The ρ-T curves for films of different thicknesses are shown in Figure 4(a). Strikingly, the 15 nm and 30 nm films show a MIT at 250 K and 204 K respectively, which is consistent

with T_C. However, the 95 nm film shows a semiconducting-like behaviour. For x=0.1, bulk $La_{0.9}Sr_{0.1}MnO_3$ is a FM insulator. One of the striking result is that thinner $La_{0.9}Sr_{0.1}MnO_3$ films with in-plane compressive strain show FM coupling with clear MIT. Density functional theory has shown that that in-plane compressive strain induces oxygen octahedrons tilt and straightens the out-of-plane O-Mn-O chain which promote MIT.[43] Figure 4(b) shows ρ-T curves measured in magnetic fields. A resistivity upturn was observed at lower temperatures of 112 K and 90 K for the 15 nm and 30 nm films, respectively (Figure S2). A similar transition in bulk at 127 K was attributed to charge/orbital ordering effect.[21] In bulk $La_{0.9}Sr_{0.1}MnO_3$, it was found that pressure reduces the resistivity and enhances T_{CO}.[44] This is consistent with our results that the thinner films with larger stain exhibit higher T_{CO} and lower resistivity. Figure 4(c) shows the magnetoresistance (MR) of the 15 nm film at different magnetic fields, defined as MR (%) = $(\rho_H - \rho_0)/\rho_0 \times 100$, where ρ_0 and ρ_H are the film's resistivities at zero and applied magnetic field (H). The MR curves show a peak value at T_{MI}, which is consistent with manganite films close to the optimum doping. In the 15 nm film, the peak MR were 38%, 70% and 81% for applied fields of 1 T, 3 T and 5 T, respectively. The difference is that thinner $La_{0.9}Sr_{0.1}MnO_3$ films show a second MR peak near T_{CO}, which is absent in optimum doped manganite films. Therefore, tuning MR near T_{CO} is a feasible approach to broaden the MR temperature range. The MR curves for films with different thicknesses are shown in Figure 4(d). The maximum MR increases with decreasing thickness. The peak MR (1 T) values are 38%, 34%, and 19% for 15 nm, 30 nm and 95 nm films, respectively.

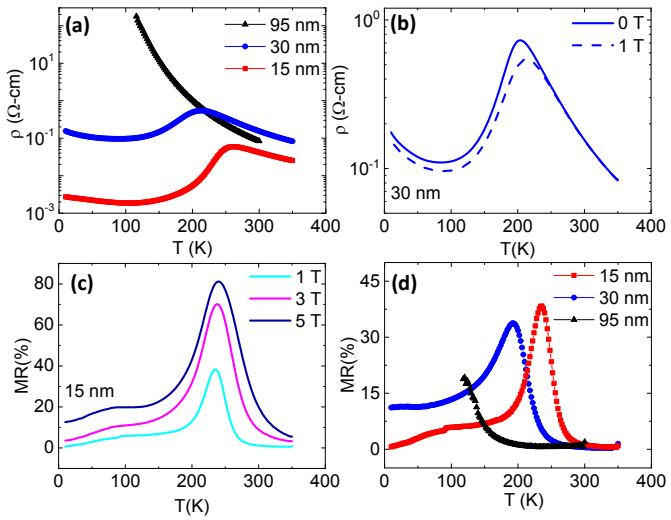

Figure 4. (a) ρ-T curves for LSMO thin films with different thicknesses. (b) ρ-T curves for the 30 nm film at a magnetic field of 0 T and 1 T. (c) MR for the 15 nm film at different magnetic fields. (d) Magnetoresistance measured at 1 T magnetic field for 15 nm, 30 nm and 95 nm films.

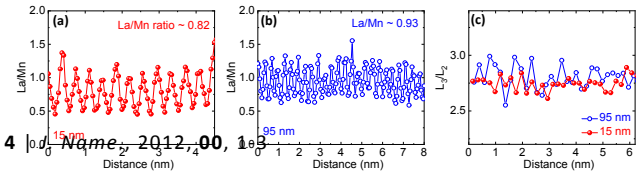

Figure 5. Position dependent La/Mn ratio from EELS results for (a) the 15 nm films and (b) the 95 nm film. (c) Position dependent Mn L_3/L_2 ratio for the 15 nm (red) and 95 nm LSMO films.

To investigate the cation stoichiometry and Mn valence states, EELS measurements of La, Mn and O were collected as shown in Figure S3a. The position dependent La, Mn and O atomic ratios are plotted in Figures S3b-S3d. The position dependent La/Mn ratios for 15 nm and 95 nm films on LAO are summarized in Figures 5a and 5b. The average La/Mn ratio is 0.83±0.06 for the 15 nm film and the average La/Mn ratio is 0.93±0.03 for the 95 nm film in both the interface and the bulk film part. The calculated Mn L_3/L_2 ratio in 15 nm film (~2.7) is slightly smaller than that in the 95 nm film (~2.8). It was reported that the Mn L_3/L_2 ratio is dependent on the Mn valence state and local coordination.[45] The larger Mn L_3/L_2 ratio indicates smaller Mn valence state. This is consistent with the La/Mn ratio in Figures 5a and 5b. It should be noted that such La/Mn ratios estimated from EELS (Figures 5a and 5b) are not absolute values as the electron channeling effects produce a nonlinear relation between signal intensity and composition, but the ratio still provides relative comparison. For example, the relative smaller La/Mn value and higher Mn valence states in the 15 nm film indicates cation off-stoichiometry, e.g., La deficiency. As discussed, a tiny change of cation composition in lightly doped manganite perovskites significantly modifies the Mn valence states and T_C. The cation stoichiometry modulation in the thinner LSMO thin films could be related to strain relaxation including both shear strain and misfit strain. For the thinner (15 nm) film, strain relaxation is accommodated by both misfit dislocations and La deficiency. During the thin film synthesis, materials often change cation stoichiometry to accommodate strain effect. For example, strain modulated stoichiometry has been also reported in vertical nanocomposites.[46, 47] Since the magnetism and transport properties in lightly doped manganites are extremely sensitive to the cation stoichiometry as discussed above, the significantly enhanced functional properties in these thinner films should be attributed to both epitaxial strain and cation off-stoichiometry effects. For thick films, strain is relaxed via misfit dislocations and microstructure modulation (e.g., tilted twin domains formation). Interfacial octahedral rotation and tilt have also been widely considered in perovskite oxide heterostructures.[48-51] Although interfacial octahedral coupling length is related to the rigidity of the octahedral network, such an interfacial effect is often believed to be effective within the first 8 unit cells or so. Therefore, such interfacial is not the dominating factor for the T_C enhancement in these 15-30 nm films.

3. Conclusion

In summary, epitaxial $La_{0.9}Sr_{0.1}MnO_3$ films of different thicknesses have been synthesized on $LaAlO_3$ substrates. Misfit dislocations at film/substrate interface are observed in thinner films while both misfit dislocations and twin domain formation are found in thicker films. The biaxial strain alone in thinner films cannot explain the greatly enhanced magnetic and transport properties. EELS results have confirmed stronger cation off-stoichiometry in the 15 nm LSMO

This journal is © The Royal Society of Chemistry 20xx

than that of the 95 nm film. Our results have demonstrated that both biaxial epitaxial strain and cation stoichiometry play critical roles in controlling magnetism and transport of lightly doped manganite films at the vertical phase boundary region.

4. Experimental section

The ceramic $La_{0.9}Sr_{0.1}MnO_3$ target was fabricated by conventional solid-state reaction method using La_2O_3 (99.99%), Mn_2O_3 (98%), and $SrCO_3$ (99%). The resulting compound was calcined at 1200 °C for 3 hours and sintered at 1450 °C for 3 hours in air. $La_{0.9}Sr_{0.1}MnO_3$ thin films were deposited on $LaAlO_3$ (001) substrates via pulsed laser deposition (PLD). Throughout all depositions, substrate temperature and oxygen pressure were maintained at 725 °C and 100 mTorr, respectively. A KrF Excimer laser (λ = 248 nm) with an energy density of 1.5 J/cm^2 and a frequency of 1 Hz was incident on the ceramic target. The substrate-target distance is 5.0 cm and the growth rate is 0.475 Å/pulse. Immediately following thin film deposition, the oxygen pressure was increased to 550 Torr, then cooled at 5 °C/min to 500 °C. The films were held for 30 minutes at this temperature to reduce oxygen deficiency. The films were then cooled to room temperature at 5 °C/min. Microstructure characterization was carried out via 2ϑ-ω measurements and Reciprocal Space Mapping in a Panalytical X'Pert Pro MRD diffractometer. AC Magnetization and resistivity data was measured in a Physical Property Measurement System (PPMS, Quantum Design). AC Magnetization data was measured by applying magnetic field parallel to film surface (in-plane). χ'-T curves were collected during cooling down from 300 K to 10 K with an AC field of 10 Oe at 5 kHz. Resistivity-temperature (ρ-T) measurements were conducted in PPMS with four Au bars sputtered onto film surface with different magnetic fields. ρ-T curves were measured as temperature was scanned from 350 K to 10 K with a scan rate of 2 K/min. A transport current of 10 mA was used. The cross-sectional TEM specimens were prepared using focused ion beam milling with a Ga ion beam at 30 kV beam energy on an FEI versa 3D workstation, followed by thinning with Ar ion milling in a Bal-Tec Res-120 ion beam milling system. The HAADF-STEM imaging and STEM-EELS elemental mapping experiments were carried out at 200 kV with an ARM200CF microscope equipped with a cold field emission electron gun, a probe Cs corrector and quantum EELS system. The chemical composition analysis and GPA are conducted by the plugin scripts in Digital Micrography software.

Acknowledgments

The work at Los Alamos National Laboratory was supported by the NNSA's Laboratory Directed Research and Development Program and was performed, in part, at the Center for Integrated Nanotechnologies, an Office of Science User Facility operated for the U.S. Department of Energy Office of Science. Los Alamos National Laboratory, an affirmative action equal opportunity employer, is managed by Triad National Security, LLC for the U.S. Department of Energy's NNSA, under contract 89233218CNA000001. S. J. Pennycook is grateful to the National University of Singapore for funding. E. Fohtung acknowledges the support from the US Department of Defense, Air Force Office of Scientific Research under Award No. FA9550-18-1-0196.

Conflicts of interest

There are no conflicts to declare.

References

1. K. J. Choi, M. Biegalski, Y. L. Li, A. Sharan, J. Schubert, R. Uecker, P. Reiche, Y. B. Chen, X. Q. Pan, V. Gopalan, L. Q. Chen, D. G. Schlom and C. B. Eom, *Science*, 2004, **306**, 1005-1009.
2. R. J. Zeches, M. D. Rossell, J. X. Zhang, A. J. Hatt, Q. He, C. H. Yang, A. Kumar, C. H. Wang, A. Melville, C. Adamo, G. Sheng, Y. H. Chu, J. F. Ihlefeld, R. Erni, C. Ederer, V. Gopalan, L. Q. Chen, D. G. Schlom, N. A. Spaldin, L. W. Martin and R. Ramesh, *Science*, 2009, **326**, 977-980.
3. D. G. Schlom, L. Q. Chen, C. B. Eom, K. M. Rabe, S. K. Streiffer and J. M. Triscone, *Annu. Rev. Mater. Res.*, 2007, **37**, 589-626.
4. A. Urushibara, Y. Moritomo, T. Arima, A. Asamitsu, G. Kido and Y. Tokura, *Phys. Rev. B*, 1995, **51**, 14103-14109.
5. A. P. Ramirez, S. W. Cheong and P. Schiffer, *J. Appl. Phys.*, 1997, **81**, 5337-5342.
6. F. S. Razavi, G. Gross, H. U. Habermeier, O. Lebedev, S. Amelinckx, G. Van Tendeloo and A. Vigliante, *Appl. Phys. Lett.*, 2000, **76**, 155-157.
7. F. Tsui, M. C. Smoak, T. K. Nath and C. B. Eom, *Appl. Phys. Lett.*, 2000, **76**, 2421-2423.
8. Y. Suzuki, H. Y. Hwang, S. W. Cheong and R. B. vanDover, *Appl. Phys. Lett.*, 1997, **71**, 140-142.
9. H. S. Wang and Q. Li, *Appl. Phys. Lett.*, 1998, **73**, 2360-2362.
10. A. P. Chen, J.-M. Hu, P. Lu, T. N. Yang, W. Zhang, L. Li, T. Ahmed, E. Enriquez, M. Weigand, Q. Su, H. Y. Wang, J.-X. Zhu, J. L. MacManus-Driscoll, L. Q. Chen, D. Yarotski and Q. X. Jia, *Sci. Adv.*, 2016, **2**, e1600245.
11. R. Groenen, J. Smit, K. Orsel, A. Vailionis, B. Bastiaens, M. Huijben, K. Boller, G. Rijnders and G. Koster, *APL Mater.*, 2015, **3**, 070701.
12. A. P. Chen, F. Khatkhatay, W. Zhang, C. Jacob, L. Jiao and H. Y. Wang, *J. Appl. Phys.*, 2013, **114**, 124101.
13. J. R. Petrie, C. Mitra, H. Jeen, W. S. Choi, T. L. Meyer, F. A. Reboredo, J. W. Freeland, G. Eres and H. N. Lee, *Adv. Funct. Mater.*, 2016, **26**, 1564-1570.
14. A. P. Chen, Q. Su, H. Han, E. Enriquez and Q. X. Jia, *Adv. Mater.*, 2019, **31**, 1803241.
15. D. E. Cox, T. Iglesias, E. Moshopoulou, K. Hirota, K. Takahashi and Y. Endoh, *Phys. Rev. B*, 2001, **64**, 024431.
16. Y. Endoh, K. Hirota, S. Ishihara, S. Okamoto, Y. Murakami, A. Nishizawa, T. Fukuda, H. Kimura, H. Nojiri, K. Kaneko and S. Maekawa, *Phys. Rev. Lett.*, 1999, **82**, 4328-4331.
17. V. E. Arkhipov, V. S. Gaviko, A. V. Korolyov, V. E. Naish, V. V. Marchenkov, Y. M. Mukovskii, S. G. Karabashev, D. A. Shulyatev and A. A. Arsenov, *J. Magn. Magn. Mater.*, 1999, **196-197**, 539-540.
18. J. Geck, P. Wochner, S. Kiele, R. Klingeler, P. Reutler, A. Revcolevschi and B. Büchner, *Phys. Rev. Lett.*, 2005, **95**, 236401.
19. S. Q. Shen, R. Y. Gu, Q. H. Wang, Z. D. Wang and X. C. Xie, *Phys. Rev. B*, 2000, **62**, 5829-5833.

20. J. S. Zhou, G. L. Liu and J. B. Goodenough, *Phys. Rev. B*, 2001, **63**, 172416.
21. R. Senis, V. Laukhin, B. Martinez, J. Fontcuberta, X. Obradors, A. A. Arsenov and Y. M. Mukovskii, *Phys. Rev. B*, 1998, **57**, 14680-14683.
22. F. S. Razavi, G. V. S. Rao, H. Jalili and H. U. Habermeier, *Appl. Phys. Lett.*, 2006, **88**, 174103.
23. R. Prasad, A. Gaur, P. K. Siwach, G. D. Varma, A. Kaur and H. K. Singh, *J. Phys. D. Appl. Phys.*, 2007, **40**, 2954-2960.
24. R. Prasad, M. P. Singh, W. Prellier, P. K. Siwach, R. Rawat, A. Kaur and H. K. Singh, *Phys. Status Solidi B*, 2009, **246**, 1662-1673.
25. J. H. Liao, W. Y. Chang, R. J. Lin and T. B. Wu, *J. Phys. D. Appl. Phys.*, 2007, **40**, 7625-7628.
26. L. Yin, C. B. Wang, Q. Shen and L. M. Zhang, *RSC Adv.*, 2016, **6**, 96093-96102.
27. H. N. Lee, S. S. A. Seo, W. S. Choi and C. M. Rouleau, *Sci. Rep.*, 2016, **6**, 19941.
28. J. Zhang, H. Tanaka, T. Kanki, J. H. Choi and T. Kawai, *Phys Rev B*, 2001, **64**, 184404.
29. W. W. Li, J. E. Kleibeuker, R. Wu, K. H. L. Zhang, C. Yun and J. L. MacManus-Driscoll, *Phys Rev B*, 2017, **96**, 165103.
30. J. Rodriguez-Carvajal, M. Hennion, F. Moussa, A. H. Moudden, L. Pinsard and A. Revcolevschi, *Phys. Rev. B*, 1998, **57**, R3189-R3192.
31. U. Gebhardt, N. V. Kasper, A. Vigliante, P. Wochner, H. Dosch, F. S. Razavi and H. U. Habermeier, *Phys. Rev. Lett.*, 2007, **98**, 096101.
32. N. Farag, M. Bobeth, W. Pompe, A. E. Romanov and J. S. Speck, *J. Appl. Phys.*, 2005, **97**, 113516.
33. J. Santiso, L. Balcells, Z. Konstantinovic, J. Roqueta, P. Ferrer, A. Pomar, B. Martinez and F. Sandiumenge, *Crystengcomm*, 2013, **15**, 3908-3918.
34. F. Sandiumenge, J. Santiso, L. Balcells, Z. Konstantinovic, J. Roqueta, A. Pomar, J. P. Espinos and B. Martinez, *Phys. Rev. Lett.*, 2013, **110**, 107206.
35. C. Adamo, X. Ke, H. Q. Wang, H. L. Xin, T. Heeg, M. E. Hawley, W. Zander, J. Schubert, P. Schiffer, D. A. Muller, L. Maritato and D. G. Schlom, *Appl. Phys. Lett.*, 2009, **95**, 112504.
36. O. I. Lebedev, G. Van Tendeloo, S. Amelinckx, F. Razavi and H. U. Habermeier, *Philos. Mag. A*, 2001, **81**, 797-824.
37. H. J. Liu, P. Yang, K. Yao and J. Wang, *Appl. Phys. Lett.*, 2010, **96**, 012901.
38. S. W. Jin, G. Y. Gao, Z. Huang, Z. Z. Yin, X. Zheng and W. Wu, *Appl. Phys. Lett.*, 2008, **92**, 261901.
39. Y. Y. Zhu, A. P. Chen, H. H. Zhou, W. R. Zhang, J. Narayan, J. L. MacManus-Driscoll, Q. X. Jia and H. Y. Wang, *APL Mater.*, 2013, **1**, 050702.
40. E. K. H. Salje, M. Alexe, S. Kustov, M. C. Weber, J. Schiemer, G. F. Nataf and J. Kreisel, *Sci. Rep.*, 2016, **6**, 27193.
41. A. J. Millis, T. Darling and A. Migliori, *J. Appl. Phys.*, 1998, **83**, 1588-1591.
42. I. C. Infante, F. Sanchez, J. Fontcuberta, M. Wojcik, E. Jedryka, S. Estrade, F. Peiro, J. Arbiol, V. Laukhin and J. P. Espinos, *Phys. Rev. B*, 2007, **76**, 224415.
43. C. G. Zhong, X. L. Lu, Y. C. Wan, Y. Min, Z. Y. Zhao, P. X. Zhou, Z. C. Dong and J. M. Liu, *J. Magn. Magn. Mater.*, 2018, **466**, 406-410.
44. V. G. Tissen, E. G. Ponyatovskii, M. V. Nefedova, V. Laukhin, B. Martinez, J. Fontcuberta, A. A. Arsenov and Y. M. Mukovskii, *J. Magn. Magn. Mater.*, 2000, **211**, 145-149.
45. H. Y. Tan, J. Verbeeck, A. Abakumov and G. Van Tendeloo, *Ultramicroscopy*, 2012, **116**, 24-33.
46. P. Lu, E. Romero, S. Lee, J. L. MacManus-Driscoll and Q. X. Jia, *Microsc. Microanal.*, 2014, **20**, 1782-1790.
47. D. Zhou, W. Sigle, E. Okunishi, Y. Wang, M. Kelsch, H. U. Habermeier and P. A. van Aken, *APL Mater.*, 2014, **2**, 127301.
48. J. He, A. Borisevich, S. V. Kalinin, S. J. Pennycook and S. T. Pantelides, *Phys Rev Lett*, 2010, **105**, 227203.
49. J. M. Rondinelli and N. A. Spaldin, *Phys Rev B*, 2010, **82**, 113402.
50. S. May, C. Smith, J.-W. Kim, E. Karapetrova, A. Bhattacharya and P. Ryan, *Phys Rev B*, 2011, **83**, 153411.
51. J. M. Rondinelli, S. J. May and J. W. Freeland, *Mrs Bull*, 2012, **37**, 261-270.

This journal is © The Royal Society of Chemistry 20xx